Journal of CO_2 Utilization 29 (2019) 65–73

Contents lists available at ScienceDirect

Journal of CO_2 Utilization

journal homepage: www.elsevier.com/locate/jcou

Low temperature water vapor pressure swing for the regeneration of adsorbents for CO_2 enrichment in greenhouses via direct air capture

Rafael Rodríguez-Mosqueda*, Job Rutgers, Eddy A. Bramer, Gerrit Brem

Department of Thermal Engineering, Faculty of Engineering Technology, University of Twente, P.O. Box 217, 7500 AE, Enschede, the Netherlands

ARTICLE INFO

Key words:
CO_2 capture
Air
Desorption
Greenhouse
Potassium carbonate
Sodium carbonate

ABSTRACT

CO_2 enrichment in greenhouses can be achieved by extracting CO_2 from the outside air. For this purpose, adsorbents based on Na_2CO_3 or K_2CO_3 are promising for trapping and releasing atmospheric CO_2. Even though the CO_2 capture by these adsorbents has been studied before, there is not much information about their regeneration at low temperatures and using air as flushing gas. In this work an experimental design study has been performed to understand the effect of temperature, water vapor pressure and air flow rate on CO_2 desorption. The results show that K-based adsorbents are a more attractive option given their higher CO_2 capture capacity and lower energy consumption compared to the Na-based ones. The estimated amount of K-based adsorbent with a capture capacity of 0.1 mmol CO_2/g_{ads} and regenerated at 50 °C with 90 mbar H_2O would occupy only 2% of the total volume contained in a closed greenhouse, fulfilling its daily CO_2 demand.

1. Introduction

The interest in capturing CO_2 directly from ambient air has considerably increased in recent years, although it is recognized that this technology cannot be the sole solution for the alarming and still increasing global problem of the elevated CO_2 concentration in the atmosphere. In one of the most ambitious applications, CO_2 harvested from ambient air can be used as carbon source for the synthesis of hydrocarbons where the hydrogen is derived from a renewable source, such as solar or wind energy. In general, the whole process of gathering large amounts of atmospheric CO_2 to its conversion into hydrocarbons such as methanol [1], still requires important breakthroughs to become a feasible technology. It is a challenge to find interesting applications that are economically feasible to make use of atmospheric CO_2. One of these might be the CO_2 enrichment in greenhouses as has been reported that keeping the indoor CO_2 concentration in the range of 1000 to 1500 ppm is optimal for the vegetable growth [2].

A common way of supplying CO_2 to greenhouses is via the burning of natural gas, alternatively combustion of biomass has also been proposed as a renewable CO_2 source. Nevertheless, these processes have the disadvantage related to the emission of toxic byproducts such as CO, NO_x, SO_x, and in the case of biomass, other volatile organic compounds as well [3]. Therefore, the CO_2 stream should be purified before it can be safely fed to the greenhouse. Another concern is the high temperature of the combustion gas, which has to be cooled down to a temperature optimum for the greenhouse [4].

CO_2 capture from ambient air and its subsequent release inside a greenhouse is an alternative to fulfill the CO_2 enrichment. Solid adsorbents appear to be the most promising alternative for capturing atmospheric CO_2 as their handling is easier than of aqueous solutions. Amine-based adsorbents have been reported to reach the highest CO_2 capture capacities [5–9], nevertheless alkaline carbonates are an interesting option since they can result in cheaper adsorbents with less environmental issues as some amines can evaporate or form hazardous byproducts. The CO_2 capture from dilute streams by potassium or sodium carbonates has been studied previously [10–15], but their regeneration has not been studied in detail. Their advantage is that they can, in principle, be regenerated at relatively low temperatures, below 100 °C, by forming a hydrated carbonate, such as sodium carbonate monohydrate ($Na_2CO_3{\cdot}H_2O$) or potassium carbonate sesquihydrate ($K_2CO_3{\cdot}1.5H_2O$). The chemical reactions proposed for the cycling between the CO_2 adsorption and desorption steps are:

$$2NaHCO_3 \leftrightarrow Na_2CO_3{\cdot}H_2O + CO_{2\,(g)} \quad \text{R1}$$

$$2KHCO_3 + 0.5\ H_2O_{(g)} \leftrightarrow K_2CO_3{\cdot}1.5\ H_2O + CO_{2\,(g)} \quad \text{R2}$$

The advantage of regenerating the hydrated carbonates rather than the anhydrous lies in the fact that the formation of the hydrates occurs at lower temperatures, which opens the possibility of supplying the heat demand for the conversion with low temperature heat.

The application proposed for these adsorbents in a system for the

* Corresponding author.
E-mail address: rf.rodmos@outlook.com (R. Rodríguez-Mosqueda).

https://doi.org/10.1016/j.jcou.2018.11.010
Received 3 October 2018; Received in revised form 14 November 2018; Accepted 26 November 2018
Available online 30 November 2018

CO_2 enrichment inside a greenhouse is comprised of a first step where the adsorbent is loaded with CO_2 by flushing it with ambient air from the environment around the greenhouse. Once the adsorption step is finished, the CO_2 desorption step is carried out by heating the adsorbent and flushing it with air from inside the greenhouse added with extra water vapor. The gas product is delivered inside the greenhouse, this way increasing the net amount of CO_2 indoors.

In this work, the type of adsorbent used is a filter with the shape of a honeycomb that is coated with Na_2CO_3 or K_2CO_3. The prime advantage of using a honeycomb structure is its very low pressure drop, which is especially important for the capture of atmospheric CO_2, given the very large volumes of air needed to pass through the adsorbent. We have previously reported results over the CO_2 adsorption step with this type of adsorbents [16,17]. Nevertheless, no data is available about their regeneration under mild conditions, i.e. below 100 °C and using air for flushing. The interaction of the adsorbents with water vapor at different relative humidities has shown to be closely linked to the CO_2 capture process. A method of experimental design is employed in order to determine the influence of three different parameters on the CO_2 desorption, these are: the desorption temperature (T), the moisture content in the air stream (p_w) used for the flushing and the volumetric air flow rate (F). Finally, the cyclic CO_2 capture capacity is evaluated to determine the net amount of CO_2 that can be delivered per mass of adsorbent per adsorption-desorption cycle, and also to investigate the variation of the energy consumption associated with it and the adsorbent size required to fulfill the daily CO_2 demand in a greenhouse. The tests are performed under a set of conditions that are relevant for the application of CO_2 enrichment in greenhouses.

2. Materials and methods

2.1. Preparation of the adsorbents

The carriers used as support in all the adsorbents were activated carbon honeycombs with square channel size of 2 mm and a wall thickness of 0.7 mm; the pieces were cut to a size of 3 x 3 cm (11 by 11 channels) and 6 cm long. The BET surface area of the carrier material was 729 m^2/g. The wet impregnation method was used for the preparation of all samples. First, the activated carbon honeycomb carriers were dried in an oven at 100 °C for 6 h. The solutions for the washcoats were prepared with demineralized water and the salts were Na_2CO_3 (Sigma Aldrich, ≥99.5%) and K_2CO_3, (Sigma Aldrich ≥ 99.0%). The solutions were prepared in such a way that the molar concentration was kept equal to 0.9 mM. The dried carriers were completely immersed in the washcoat solutions until no more bubbling was noticed, and then they were manually shaken to remove any excess solution remaining in the channels. Finally, they were calcined in the experimental setup at 200 °C with a flow of N_2. The loadings were calculated from the weight change as W_{salt}/W_{ads}, where W_{salt} is the salt weight loaded in the adsorbent and W_{ads} is the total adsorbent weight, that is $W_{ads} = W_{salt} + W_{carrier}$. Table 1 presents information about the prepared adsorbents and the test runs carried out.

2.2. Experimental setup

The scheme of the experimental setup is shown in Fig. 1. It consists of a reactor (R1) of square cross-section with dimensions 5 × 5 x 20 cm, while the gas is fed at the bottom of it. The monolithic adsorbent is placed on top of a metal foam to ensure a uniform flow distribution. Two thermocouples are inserted from the top of the reactor as depicted in the right-hand side in Fig. 1. The thermocouples reach different depths in the honeycomb, at the middle (T middle) and bottom (T bottom) parts of it. The gas stream fed to the reactor varied among experiments from N_2 to air with 400 ppm of CO_2, either dry or humid. The air stream was prepared by passing dry air at a pressure of 5 bar through column C1, filled with zeolite 13X beads that removed all CO_2 in it; except for the CO_2 capture cyclic experiments, for those dry air from the grid without further CO_2 addition was fed directly to the reactor. The flow coming out of the column C1 was divided into two streams, controlled by flow controllers FC2 and FC3. The water was added by bubbling one of these flows in the humidifier, kept at a constant temperature. The CO_2 (Linde, ≥99.7 vol-%) addition was administered using flow controller FC1. Before each experiment the gas mixture prepared was left to stabilize, meanwhile exiting the system from valve V1 located just before the reactor. Once the gas mixture remained stable, valve V1 was switched, feeding the reactor and the experiment was started. The concentration of CO_2 and H_2O in the feed stream were measured using sensor S1 (PP Systems SBA-5 CO_2) and sensor S2 (Omega HX92 A coupled with a thermocouple), respectively. The CO_2 content in the stream exiting the reactor was measured with sensor S4 (LI-COR LI-820). The humidity content in the stream exiting the reactor was measured at two points: immediately after the reactor with sensor S3 (Omega HX92 A coupled with a thermocouple), and after the condenser by means of sensor S5 (PP systems SBA-5 CO_2/H_2O). The total volumetric flow rate was measured at the exhaust by means of flowmeter FM (DryCal Mesa Labs Defender 520). Calibration of the CO_2 sensors was checked throughout the experimental set.

2.3. Equilibrium of adsorption of water by the adsorbents

We have previously reported the equilibrium of adsorption of water by the carrier material as well as by Na- and K-based adsorbents with salt loadings similar to the ones employed in this work [16,17]. Data was gathered from those works and completed with extra experiments when necessary. The samples were exposed to ramps of relative humidity (RH) at different temperatures (20, 30 and 40 °C) using N_2 as sweeping gas; the weight change after reaching equilibrium was used to determine the amount of water adsorbed or desorbed. The experimental data was fitted to the model proposed by Do et al. [18] for the adsorption of water by activated carbons.

2.4. CO_2 desorption tests. Design of experiments

A complete CO_2 capture cycle from the design of experiments sets was comprised of the following steps: hydration, CO_2 adsorption, CO_2 desorption and calcination. The hydration step is to hydrate the salt and load the adsorbent with water, and the calcination step is to completely regenerate the adsorbent. Table 2 shows the conditions used for the

Table 1
Preparation of the adsorbents and tests run with each sample.

Adsorbent	Washcoat solution [g_{salt}/g_{water}]	Loading [g_{salt}/g_{ads}]	Bulk density [Kg/m^3]	Experiment runs
Na	0.096	0.051	409	Design of exp. 1st block Cyclic tests
K-1	0.125	0.052	410	Design of exp. 1st block
K-2	0.125	0.048	404	Design of exp. 2nd block Cyclic tests

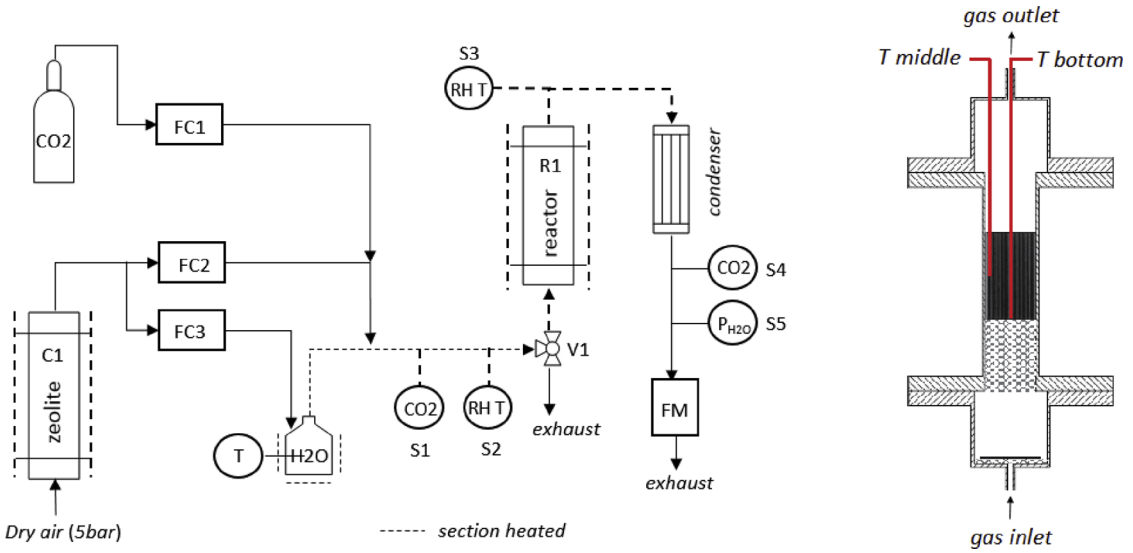

Fig. 1. Diagram of the experimental setup (left) and location of the thermocouples inside the reactor (right).

Table 2
Experimental conditions of the hydration, CO_2 adsorption and calcination steps.

Experiment	T [°C]	p_w [mbar]	F [L/min]	RH	gas
Hydration	30	30	5	72 %	N_2
CO_2 adsorption	30	12	15	26 %	Air 400 ppm CO_2
Calcination	210	0	5	0 %	N_2

hydration, CO_2 adsorption and calcination steps. The CO_2 desorption tests were performed varying the values of three factors: temperature (T), H_2O content in the air stream (p_w) and the volumetric dry air flow rate (F). The experimental factors were varied in the ranges of: T: 50 to 80 °C; p_w: 40 to 90 mbar; and F: 3 to 5 L/min. Specifically for the CO_2 desorption steps from the design of experiments sets, there was a pre-heating phase where the adsorbent was heated to the required desorption temperature without any gas flush. When the adsorbent was at the desired set point temperature and the prepared gas remained stable, the experiment was started by switching valve V1 before the reactor (see Fig. 1).

The whole matrix of experimental conditions was not examined, but only a fraction of the total runs accordingly to the design of experiments method employed. The design method and the subsequent statistical analysis of the results were done using Minitab® Statistical Software. The lists of conditions of all performed desorption tests are given in Table S1 and Table S2 in the Supporting Information. The K-based adsorbents required an extension of the number of tested conditions due to non-linearity of the results. The condition with the three factors at their middle value (65 °C, 65 mbar and 4 L/min) was performed multiple times per block to assess the repeatability and curvature in the response variable. The response variable chosen for computing the statistical analysis was the CO_2 desorption yield. The CO_2 desorption yield, $Y_{CO2,}$ is the ratio of the accumulative amount of CO_2 released in time during the desorption step, n_{CO2des} (t), divided by the total amount of CO_2 captured during the previous adsorption step, n_{CO2ads}. It indicates the extent of regeneration of the adsorbent. It is calculated according to equation Eq (1).

$$Y_{CO2} = \frac{n_{CO2\,des}(t)}{n_{CO2\,ads}} \quad (1)$$

2.5. X-ray diffraction tests

Some of the sorbent products from the desorption tests were analyzed with X-ray diffraction using a PANalytical X'Pert Pro Powder diffractometer equipped with a copper anode X-ray tube; Joint Committee Powder Diffraction Standards (JCPDS) were used for the phase identification.

2.6. CO_2 capture cyclic tests

Cyclic tests were performed by running adsorption and desorption steps continuously. The adsorption step was performed at the same conditions given in Table 2. Once the outlet CO_2 level equaled the inlet value, the adsorption step was stopped and the experimental setup was set into the desorption mode. For this, the volumetric flow rate of air was reduced from 15 L/min (used for the adsorption step) to 5 L/min; the reactor and the humidifier were set to heating ramps up to the desorption temperature and dew point desired, respectively. The desorption conditions used for these tests were chosen from the results of the design of experiments. When the CO_2 concentration remained stable and equal to the inlet value, the desorption was finished and the next adsorption step was started immediately, no cooling time was allowed between experiments.

3. Results and discussion

3.1. Equilibrium of water adsorption

Fig. 2 shows the hysteresis loops for the adsorption of water by the carrier and both the Na- and K-based adsorbents. Independently of the temperature used (20, 30 or 40 °C), the weight gain was determined by the value of the relative humidity only. The presence of the salts over the carrier increased its water adsorption due to the formation of salt hydrates or an aqueous solution. It is seen that for the part of the experiment where the relative humidity in the system was increased (solid lines) the K-based adsorbent captured more water than the Na-based, up to 70% RH. This is due to the more hygroscopic character of K_2CO_3, which is confirmed by the formation of an aqueous solution (i.e. deliquescence) above 43% RH [19], while for Na_2CO_3 this occurs roughly above 80% RH [20]. It is also noted that the hysteresis area of the Na-based adsorbent is a little bit larger than that of the K-based adsorbent. The fitting results from the Do et al model [18] show that the K-based adsorbent requires the formation of smaller water clusters to condense into the pores that the Na-based, and that the attachment of the first water molecules is more favored. On the other hand, the relaxation constant of these clusters is larger for the Na-based adsorbent,

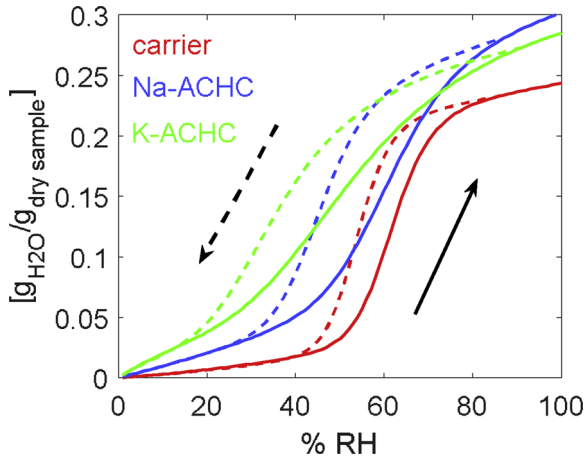

Fig. 2. H_2O adsorption by the carrier, Na- and K-based adsorbents. Increasing relative humidity path (solid line), decreasing relative humidity path (dashed line). Tests were performed at 20, 30 and 40 °C.

explaining the difference on the hysteresis area. The complete set of fitting parameters is given in Text S1 in the Supporting Information. With respect to the behavior of the adsorbents when cycled in a real application, it is proposed to run the CO_2 desorption step at a relative humidity somewhere around the plateau of water uptake. Then, part of this water will evaporate during the subsequent adsorption step depending on the humidity conditions of the ambient air at the location. This evaporation results in a local cooling which is favorable for the CO_2 adsorption.

3.2. CO_2 desorption tests. Design of experiments

Fig. 3 shows the CO_2 desorption profiles for the Na- and K-based adsorbents, the x-axis is plotted only for the first 10 min of the desorption test since more than 60% of the total CO_2 that was released in each experiment occurred in this timeframe for both adsorbents. Figure S1 in the Supporting Information shows the CO_2 desorption profile over the entire time length.

The CO_2 concentration depends on the amount of adsorbent and thus on the reactor size for a given air flow rate. Therefore, the values obtained here can be taken as lower boundary levels.

The experiments run with the lowest flow rate of 3 L/min led to higher CO_2 concentrations due to lower dilution effects. It is noticed that the Na-based adsorbents reached higher CO_2 concentrations compared to the K-based ones, roughly 15 000 vs 10 000 ppm. This can be explained by comparing both theoretical chemical equilibriums; Na_2CO_3 has a lower equilibrium constant for the carbonation reaction compared to K_2CO_3, or said in another way, the CO_2 desorption is favored for $NaHCO_3$ [21,22]. The average capture capacity obtained from all the CO_2 adsorption steps was 0.14 mmol CO_2/g_{ads} for the Na-based adsorbent while it was 0.23 mmol CO_2/g_{ads} that of the K-based adsorbent. The resulting salt conversion was 29% and 64%, respectively. Figure S2 shows the CO_2 adsorption capacity over the entire design of experiments set for the two adsorbents.

It is noticed in Fig. 3 that the CO_2 desorption started immediately in all cases, this was due to the pre-heating phase of the experiment with no air flush. This caused a partial CO_2 release, which stayed inside the reactor. Then, when air was flushed this loose CO_2 was released instantaneously, producing a CO_2 concentration peak at the outlet of the reactor. The higher the temperature of the desorption, the higher the initial peak of the CO_2 concentration. Nevertheless, in some cases there was a second peak seen at later times, this was observed for the experiments performed at 50 °C and 90 mbar H_2O. Once again, water adsorption plays a determinant role as this desorption condition resulted in the highest relative humidity, 72%RH (at 50 °C), from the whole set of conditions tried. Given that the adsorption step was performed at 26%RH (at 30 °C), the adsorbent re-gained the largest amount of water under this desorption condition. This led to a significant exothermic effect in both adsorbents, which was favorable for the desorption of the CO_2. Fig. 4 shows the temperature at the bottom and middle positions of the K-based adsorbent (see right-hand side of Fig. 1 to locate the position of the thermocouples). As it is shown, there was a temperature increase that continued along the length of the adsorbent as the gas became hotter and water was still adsorbed. The temperature increase at the inlet of the adsorbent channel was around 5 °C and it reached 12 °C at half its length. This exothermic effect provoked the second peak in the CO_2 desorption profiles observed for the experiments at 50 °C and 90 mbar H_2O. Oppositely, all experiments performed at 80 °C showed a considerable cooling effect, which was more pronounced for the tests at 40 mbar H_2O. This condition corresponded to a relative humidity of 9%RH.

As mentioned before, the average adsorption capacity was 0.14 mmol CO_2/g_{ads} and 0.23 mmol CO_2/g_{ads} for the Na- and K-based adsorbents, respectively. The fraction of this capacity that is regenerated during the CO_2 desorption step is represented by the desorption yield, Y_{CO2}. The desorption yield would be equal to one if all adsorbent is regenerated. Fig. 5 shows the desorption yield for the Na-

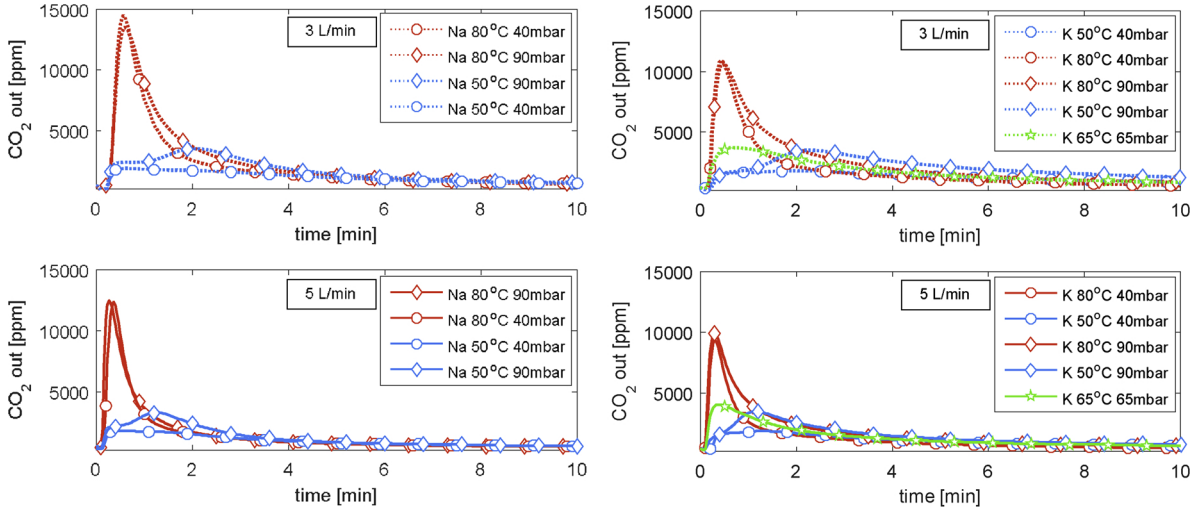

Fig. 3. CO_2 desorption profile over the first 10 min for the Na- (left) and K-based adsorbents (right) at different temperatures and water vapor pressures, grouped according to the flow rate used.

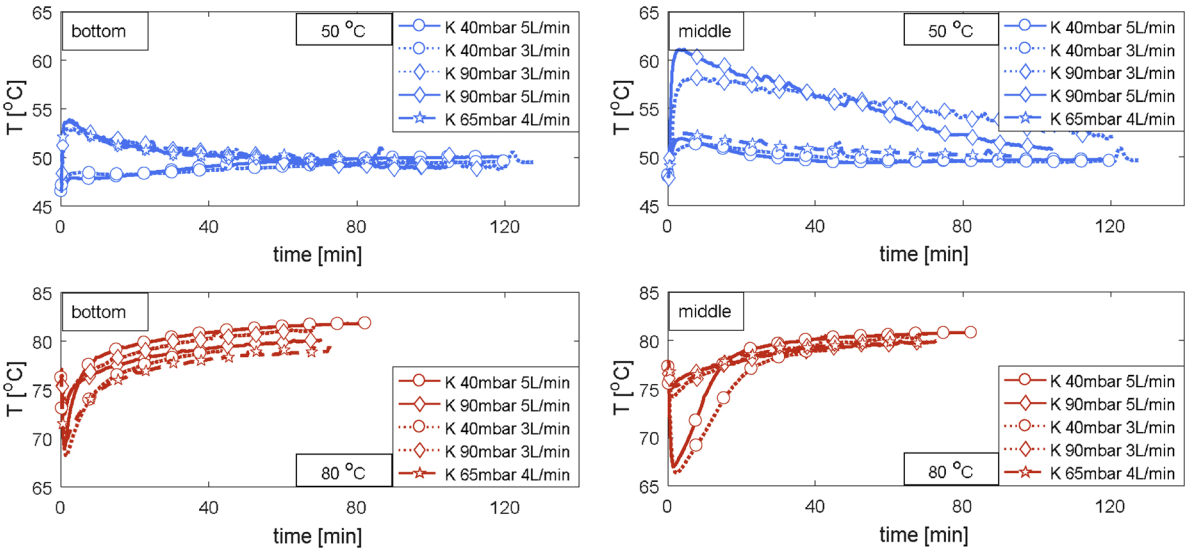

Fig. 4. Temperature at the bottom (left) and middle (right) locations for the K-based adsorbents during the CO_2 desorption at different temperatures, water vapor pressures and air flow rates.

and K-based adsorbents. It is seen in both cases that it increased with the water vapor pressure, but was hindered by increasing temperature. Regarding the flow rate, only a slight influence for the Na-based adsorbent can be observed.

The CO_2 desorption yield is the response variable used for the statistical analysis. The resulting statistical model for the Na-based adsorbent is given in equation Eq. (2), the input parameters are given in T [°C], p_w [mbar] and F [L/min].

$$Y_{CO2} = 0.1347 + 0.00425\,T + 0.00421\,p_w + 0.0456\,F - 0.00003\,T\,p_w - 0.00062\,T\,F \quad (2)$$

The standard deviation of the model is 0.00649, which represents 1% of the lowest desorption yield measured and $r^2 = 0.9924$, indicating a very good fit. Opposite to the Na-based adsorbent, the results from the K-based adsorbent could not be represented with a linear model (Block 1 in Table S2), for which extension of the conditions tested was required to tackle the curvature of the results (Block 2 in Table S2). The resulting statistical model for the K-based adsorbent is given in equation Eq. (3), the same units are used as in equation Eq. (2).

$$Y_{CO2} = 0.1781 - 0.00217\,T + 0.0099\,p_w - 0.00004\,p_w^2 \quad (3)$$

The standard deviation of the model is 0.01569, which represents 5% of the lowest desorption yield measured and $r^2 = 0.9695$, indicating a good fit.

Fig. 6 shows the response surface plots for both adsorbents. The most favorable desorption conditions are in the direction of lower temperatures and higher water vapor pressures, that is high relative humidity. High temperatures are in principle favorable for the decomposition of the bicarbonate salts, nevertheless the process can also be controlled by the water vapor pressure in the system depending on the chemical reaction path followed.

3.3. Chemical reaction path

For the case of the regeneration towards an anhydrous carbonate the chemical path goes accordingly to reaction R3 (M = Na or K), where only heat is required for the conversion to the anhydrous carbonate, but this process is favored above 100 °C for both salts [21,23].

$$2MHCO_3 \rightarrow M_2CO_3 + H_2O_{(g)} + CO_{2(g)} \quad \text{R3}$$

Alternatively, the bicarbonate can follow a different regeneration path leading to the formation of a hydrated carbonate as depicted in

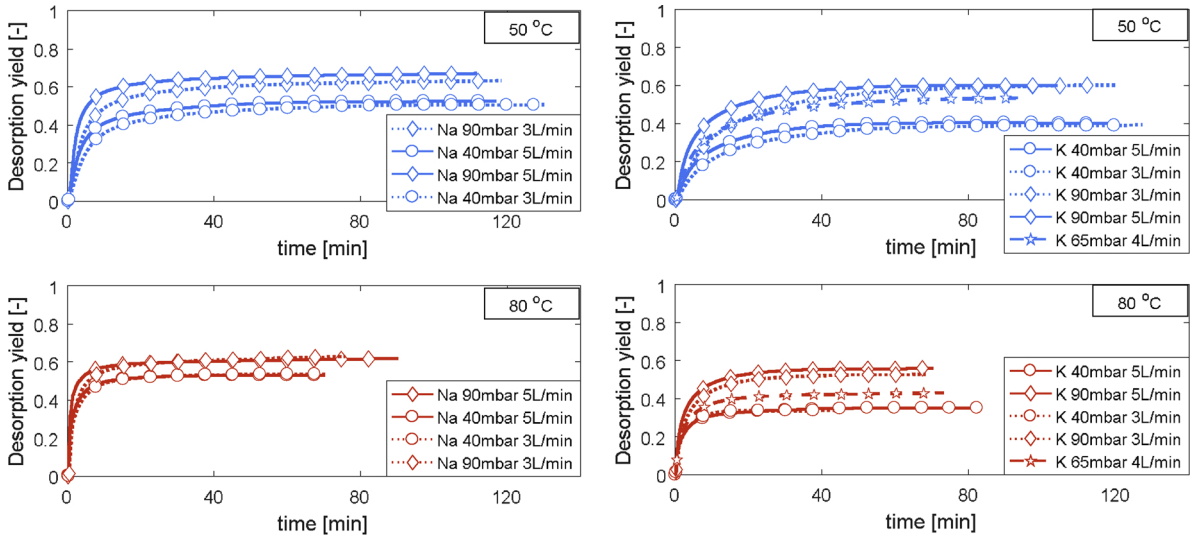

Fig. 5. Desorption yield for the Na- (left) and K-based adsorbents (right) at different temperatures, water vapor pressures and air flow rates.

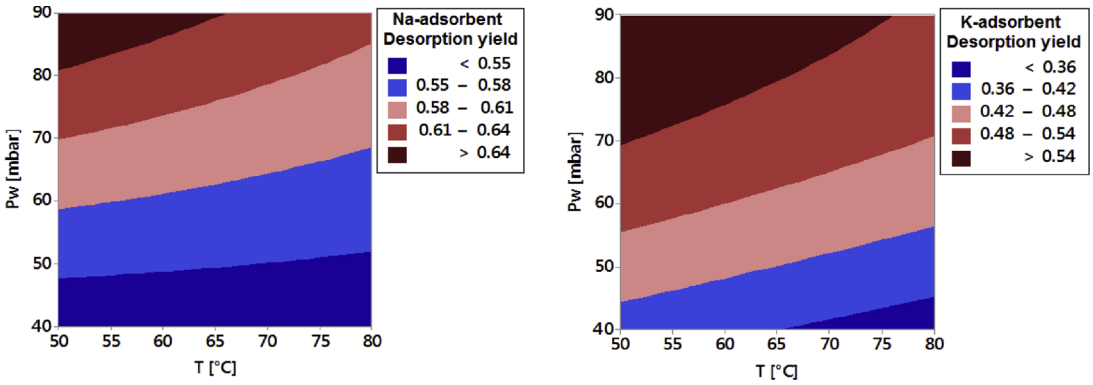

Fig. 6. Surface plots of the desorption yield for the Na- (left) and K-based adsorbents (right).

reactions R1 and R2, but these reactions only take place when the temperature and water vapor pressure conditions lie within the stability region of the corresponding hydrated carbonate. That is, the relative humidity during the desorption should not be below the minimum required for the formation of the hydrates and the temperature should not be too low that the desorption is inhibited.

Fig. 7 shows the X-ray diffraction patterns of the products from the adsorption step and after desorption at 50 °C and 90 mbar H_2O. In the case of the Na-based adsorbent the adsorption step produced $NaHCO_3$ and there was still some unreacted Na_2CO_3 and $Na_2CO_3{\cdot}H_2O$. After desorption at the optimum condition as found from the statistical analysis, the XRD pattern showed a reduction of the intensity (with respect to the baseline of each sample) of the reflection corresponding to $NaHCO_3$ while the intensity of the hydrated carbonate became stronger, indicating the conversion of the primer and the formation of the latter. For the case of the K-based adsorbent, once again the adsorption step led to the formation of $KHCO_3$ and the reflection corresponding to K_2CO_3 was very weak. After the desorption step no signals corresponding to any potassium salt were observed. The reason for this is due to the highly deliquescent character of this salt. The aqueous solution formed is not visible with XRD. The reflections corresponding to graphite and quartz are from the activated carbon carrier material.

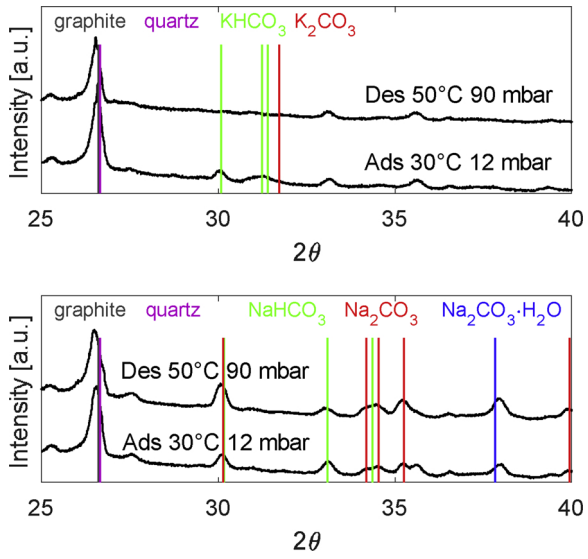

Fig. 7. X-ray diffraction patterns from the products of the adsorption step and after desorption at 50 °C and 90 mbar H_2O for the K- (up) and Na-based (down) adsorbents.

3.4. CO_2 capture cyclic tests

To further investigate the stability of the adsorbents and to determine the trends of the energy consumption and the operational CO_2 capture capacity, the adsorbents were subjected to cycles comprising continuous adsorption and desorption steps. This is important to investigate as in a real application neither a hydration or a calcination step are feasible due to the high energy requirements and the need of an oxygen-free gas for calcination at a high temperature to prevent that the carbon material is burned. The desorption conditions were chosen according to the results from the statistical models such that the desorption yield was above 0.5 (50% regeneration of the adsorbent).

The samples were the ones used for the design of experiments study (Na and K-2, see Table 1). Therefore, these adsorbents had already been subjected to around 10 cycles each. Fig. 8 shows the obtained cyclic desorption capacity under different conditions. In general, the desorption capacity was not reduced during cycling, although these are lower than the previous results for a single cycle. Recalling the average CO_2 adsorption capacity and the desorption yields obtained from the design of experiments set, the cycles run with a desorption at 50 °C and 90 mbar H_2O should have led to a desorption capacity of around 0.09 and 0.12 mmol CO_2/g_{ads} for the Na- and K-based adsorbents, respectively. The reason for the lower desorption capacities has to do with the skipping of the hydration and calcination treatments as well as the fact that the adsorption step in these experiments was immediately started after the previous desorption, that is with a heated adsorbent. Once again, the K-based adsorbent resulted in higher CO_2 desorption capacities and the highest of them was obtained at 50 °C and 90 mbar H_2O as suggested by the statistical model. Regarding the physical stability of the adsorbents, it was noticed that the surface of the Na-based adsorbent became more fragile as fine dust was easily detached from it. On the contrary the K-based adsorbent maintained its structure almost unmodified. Cycles were also performed with the K-based adsorbent at 50 °C and 25 mbar H_2O, which corresponds to a dew point of around 21 °C in the humidifier, as in that case little or no heat is required for humidifying the air stream for the flushing. The resulting CO_2 desorption capacity for this situation was the lowest, showing the importance of water addition.

3.5. Energy consumption of the desorption step

Fig. 9 shows the energy consumption per mol CO_2 for the different desorption conditions as the desorption step proceeds in time. Text S2 in the Supporting Information shows the detailed energy balance. It has been assumed that the gas used for the flushing during the desorption step is air from inside the greenhouse, with 30 °C and 50%RH, while the water reservoir providing steam for humidifying the air stream is at 20 °C. Energy is put into the system from the beginning to transport and heat the gas, but little CO_2 is released. This results in very high energy

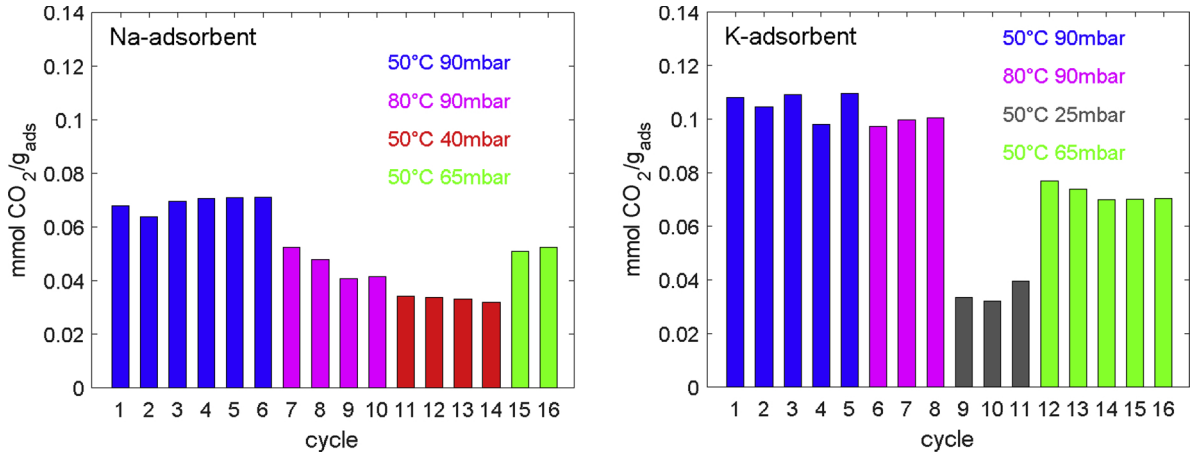

Fig. 8. Cyclic CO_2 desorption capacity for the Na- (left) and K-based (right) adsorbents at different temperatures and water vapor pressures during the desorption step.

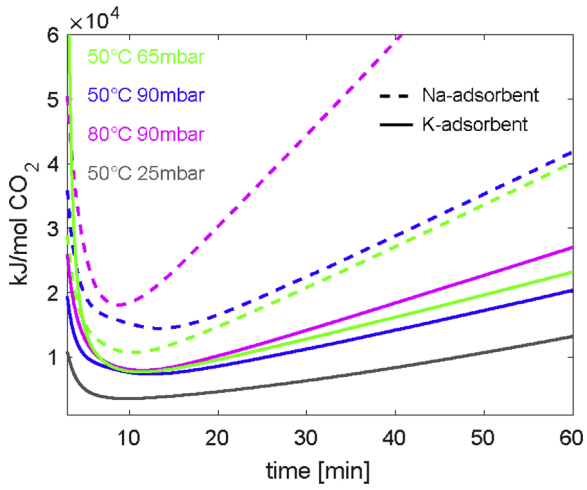

Fig. 9. Trend of the energy consumption per mol CO_2 associated with the desorption step under different temperature and water vapor pressure conditions for the Na- (dashed lines) and K-based (solid lines) adsorbents.

consumption values at the beginning of the tests. As the CO_2 desorption proceeds, the specific energy consumption reaches a minimum level and then starts to increase again. It is noted that the lines for the Na-based adsorbent are above those of the K-based, this is because of its lower CO_2 uptake. The lowest energy consumption of 3500 kJ/mol CO_2 corresponds to a desorption condition of 50 °C and 25 mbar H_2O for the K-based adsorbent. Focusing on the rest of the lines for the K-based adsorbent, it is seen that they fairly overlap when reaching the minimum value of circa 8000 kJ/mol CO_2, independently of temperature. Performing the desorption at higher temperatures (> 50 °C) can be discarded as an optimum condition since the cyclic desorption capacity was not higher at 80 °C, as it was predicted from the statistical model. Moreover, the mean energy consumption showed to be the highest at 80 °C, i.e. this line has the highest increase at longer times.

The criteria for selecting the set point of the water vapor pressure will be determined by different factors such as the availability of heat to produce the required amount of steam in the humidifier, the total energy consumption and the resulting CO_2 desorption capacity. Certainly, adding little or no heat to increase the H_2O content in the air stream results in a lower energy consumption, however the desorption capacity also drops considerably as it was only 0.04 mmol CO_2/g_{ads} for a condition of 50 °C and 25 mbar H_2O. This would require a larger amount of adsorbent in order to fulfill the CO_2 demand in a greenhouse. Heat availability can be a limiting factor to the highest reachable temperature in the humidifier depending on the type of heat source used. If the air stream leaving the humidifier is saturated with water vapor at the temperature of the humidifier, the dew points determine the temperature of the water reservoir. For a desorption condition of 65 mbar H_2O the water reservoir should be kept at around 38 °C, while for a condition of 90 mbar H_2O, the water reservoir should be heated up to 44 °C. As mentioned before, the minimum energy consumption was almost the same for the cases of 50 °C with either 65 or 90 mbar H_2O and as time proceeded the lines separated. However, contrary to what could be expected from a higher temperature requirement in the humidifier, the energy consumption per mol of CO_2 desorbed was lower for the condition of 90 mbar H_2O than with 65 mbar H_2O. The reason for this is due to the higher desorption capacity obtained at the higher water vapor pressure. Figure S3 shows the accumulative desorption capacity for the tests at 50 °C with the K-based adsorbent. When the energy consumption per mol of CO_2 was at its minimum value (circa 8000 kJ/mol CO_2), both conditions had similar desorption capacities, these were 0.04 mmol CO_2/g_{ads} with 65 mbar H_2O and 0.05 mmol CO_2/g_{ads} with 90 mbar H_2O. Nevertheless, these values are still quite low, and it can be doubled to 0.1 mmol CO_2/g_{ads} for the condition of 90 mbar H_2O, with a 25% increase of the energy consumption (around 10 000 kJ/mol CO_2). On the other hand, this same increase in the energy consumption resulted in a poorer desorption capacity of 0.06 mmol CO_2/g_{ads} for the condition of 65 mbar H_2O. The optimum water vapor pressure in a real application will depend on the specific CO_2 enrichment needs as well as on the availability of heat from a CO_2-free source.

Figure S4 shows the distribution of the energy consumption for these two desorption conditions. In both cases the energy required in the humidifier to heat the water reservoir from the initial temperature (20 °C) to the dew point plus the energy to evaporate the required amount of steam accounts for more than 70% of the total energy consumption. This suggests that most of the total energy requirements can be covered with heat from a low temperature source (≤ 44 °C). The smallest contribution to the energy consumption (≤ 5%) is destined to transport the gas through the adsorbent, and the rest of the energy (≥ 95%) is for heating purposes, evidencing that it is during the desorption step that most of the total energy is consumed in the entire process.

It is important to point out that these are not the ultimate energy consumption values in a real application, but they help in identifying and understanding the trends followed when the desorption conditions are varied.

3.6. Required adsorbent reactor volume in a greenhouse

In an open greenhouse the temperature is regulated by letting

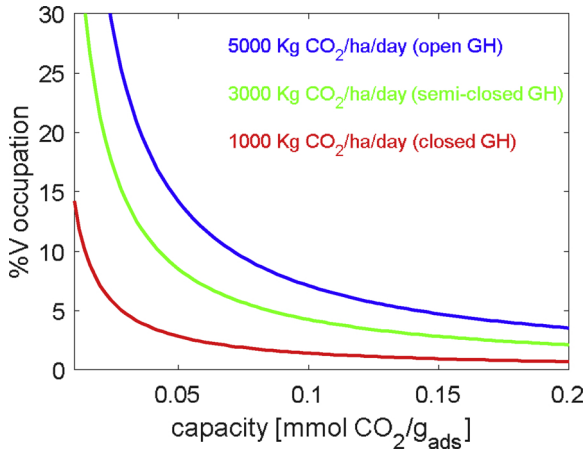

Fig. 10. Fraction of the total greenhouse volume that would be occupied by the adsorbent in function of the CO_2 desorption capacity for three different daily CO_2 supply requirements with a set point of 1000 ppm CO_2. CO_2 supply requirements taken from Qian et al. [26].

outside air to flow through the installation, while in a closed greenhouse the temperature is controlled actively via air-conditioning systems. Therefore, open greenhouses present the disadvantage that CO_2 is greatly diluted, thus the net CO_2 amount required to maintain a given concentration target is considerably higher than in a closed greenhouse where dilution is not a concern. Semi-closed greenhouses are in-between these two situations [24]. Estimates of supply rates for different type of greenhouses are used in order to calculate the size of adsorbent required for fulfilling the daily CO_2 demands. The values will vary depending on the targeted CO_2 concentration, type of vegetables grown, time of the year and leakage rate of outside air. An estimated air volume of 40,000 m^3/ha for a typical greenhouse with a gutter height of 2.4 m is used to calculate the fraction of the total volume that the required amount of adsorbent would occupy [25]. Fig. 10 shows the space occupation for covering the CO_2 demands in different types of greenhouses in function of the CO_2 desorption capacity; the CO_2 supply requirements were taken from Qian et al. [26]. The closed greenhouse case counts with an active cooling system with a duty of 700 W/m^2, this does not require outside air to flow through the greenhouse. The semi-closed greenhouse has a cooling duty of 150 W/m^2, and some outside air is required to complete the cooling task. Finally, the open greenhouse does not count with any sort of active cooling. With a desorption capacity of 0.1 mmol CO_2/g_{ads} the K-based adsorbent could fulfill the total CO_2 demand, occupying 7% of the volume of the open greenhouse case and just 1.5% in the closed greenhouse case. Nevertheless, these values should be considered as upper bound estimates since they correspond to the amount of adsorbent necessary to cover the total CO_2 demand in a single CO_2 capture cycle, i.e. one adsorption and one desorption step per day. The adsorbent size can be reduced if several CO_2 capture cycles are run per day as long as the optimum CO_2 concentration in the greenhouse is maintained. The CO_2 capture units could be distributed evenly over the area of the greenhouse so that the CO_2 is enriched uniformly.

3.7. Comparison between the Na- and K-based adsorbents with other technologies for CO_2 enrichment in greenhouses

Listing the similarities and pros and cons of both adsorbents, it was observed that the salts enhanced the H_2O adsorption of the carrier and that this had a positive effect on the CO_2 desorption. It is proposed to perform the desorption step at a high relative humidity to promote this exothermic response, however, the extent of this H_2O adsorption will be limited by the relative humidity during the previous CO_2 adsorption step, which is determined by the environmental conditions at the location. Regarding the CO_2 desorption step, the Na-based adsorbent led to higher CO_2 concentrations in the outlet gas, however, the overall desorption capacity was considerably lower compared to the K-based adsorbent. Even though, the Na-based adsorbent showed to have higher desorption yields, this did not result in a higher desorption capacity due to the lower amount of CO_2 captured. In this sense, a higher CO_2 concentration in the exhaust of the reactor is not a real advantage since the main purpose of the process is to increase the net amount of CO_2 inside the greenhouse, and thus a higher CO_2 desorption capacity is crucial. Moreover, the K-based adsorbent showed to better preserve its physical structure as no considerable damage was observed after cycling. Increasing the amount of salt loaded over the carrier would represent a big improvement. In this work higher salt loadings were tried, but they compromised the stability of the adsorbent considerably. Most of the energy consumption in the process is supplied during the desorption step, in this regard the K-based adsorbent showed to be a cheaper option.

The current technology for CO_2 enrichment in greenhouses is via the burning of natural gas, which carries different issues such as the production of toxic gases. In order to reduce the emissions of these contaminants the operational conditions of the burner need to be tuned, for instance, care has to be taken on controlling the air to fuel ratio as well as the combustion temperature in order to reduce the CO level to a minimum [27]. Also, large quantities of heat should be extracted from the flue gas to cool it down to an acceptable temperature for the greenhouse. These issues make the burning of fuels a more complex multi-stage process. The advantage of this system is that it can be coupled to the generation of electricity to cover other needs in the greenhouse. Recently, other technologies have been proposed, such as the use of CO_2 clathrate hydrate in a system that not only provides CO_2, but also acts to some extent as an air-conditioning system for the greenhouse. Nevertheless, the formation of this hydrate requires very high CO_2 pressures and temperatures close to 0 °C [28]. With respect to other CO_2 adsorbents, zeolite beads have shown to be able to increase the inner concentration in closed environments, but they perform better at rather low temperatures and their capacities are considerably lower than the rest of adsorbents tested for direct air capture, such as 0.042 mmol CO_2/g at an adsorption temperature of 5 °C [29].

The K-based adsorbents studied in this work offer the possibility of performing the CO_2 capture and CO_2 enrichment in the same reactor. Although the energy requirement appears to be large, this can be supplied by means of low temperature heat. Furthermore, no toxic emissions are associated with the operation of the system. Therefore, K-based adsorbents can be considered an attractive option for CO_2-enrichment in greenhouses.

4. Conclusions

CO_2 adsorbents comprised of Na_2CO_3 or K_2CO_3 loaded on activated carbon honeycombs are attractive candidates for use in systems to enrich the CO_2 content of air in closed greenhouses. A design of experiments study on the effect of different operational conditions on the regeneration of the adsorbents showed that for both sorbents lower temperatures and higher water vapor pressures, i.e. higher relative humidities, result in a higher CO_2 desorption capacity. This is due to the formation of hydrated carbonates which have lower reaction enthalpies than the anhydrous carbonates. On the other hand, water vapor should be supplied for these reactions to take place. K-based adsorbents appear to be more promising than Na-based due to the higher cyclic CO_2 capture capacity. The CO_2 desorption capacity is around 0.1 mmol CO_2/g_{ads} for an adsorption temperature at 30 °C and a CO_2 desorption step at 50 °C and 90 mbar H_2O. However, the CO_2 capture capacities are still low compared with those of some amine-based adsorbents proposed in literature. Nevertheless, the relatively modest net CO_2 requirements for greenhouses make K-based adsorbents a good and competitive option, since they represent minor hazardous issues in case any of the salt or

the amine is emitted out of the system due to erosion or evaporation. Moreover, the low temperature at which heat must be supplied for their regeneration can be fulfilled with low quality heat or with heat from a renewable (CO_2-free) source, such as solar heaters.

Declarations of interest

None.

Acknowledgments

Portions of information contained in this publication are printed with permission of Minitab Inc. All such material remains the exclusive property and copyright of Minitab Inc. All rights reserved. MINITAB® and all other trademarks and logos for the Company's products and services are the exclusive property of Minitab Inc. All other marks referenced remain the property of their respective owners. See minitab.com for more information.

The authors thank Ing. Henk-Jan Moed for his technical contributions.

This research did not receive any specific grant from funding agencies in the public, commercial or not-for-profit sectors.

Appendix A. Supplementary data

Supplementary material related to this article can be found, in the online version, at doi:https://doi.org/10.1016/j.jcou.2018.11.010.

References

[1] P.D. Tran, L.H. Wong, J. Barber, J.S.C. Loo, Recent advances in hybrid photocatalysts for solar fuel production, Energy Environ. Sci. 5 (3) (2012) 5902–5918.
[2] M. Xin, L. Shuang, L. Yue, G. Qinzhu, Effectiveness of gaseous CO2 fertilizer application in China's greenhouses between 1982 and 2010, J. CO2. Util. (11) (2015) 63–66.
[3] L.-M. Dion, M. Lefsrud, V. Orsat, Review of CO2 recovery methods from the exhaust gas of biomass heating systems for safe enrichment in greenhouses, Biomass Bioenergy 35 (8) (2011) 3422–3432.
[4] Y. Roy, M. Lefsrud, V. Orsat, F. Filion, J. Bouchard, Q. Nguyen, L.-M. Dion, A. Glover, E. Madadian, C.P. Lee, Biomass combustion for greenhouse carbon dioxide enrichment, Biomass Bioenergy 66 (2014) 186–196.
[5] M.A. Sakwa-Novak, C.J. Yoo, S. Tan, F. Rashidi, C.W. Jones, Poly(ethylenimine)-functionalized monolithic alumina honeycomb adsorbents for CO2 capture from air, ChemSusChem 9 (14) (2016) 1859–1868.
[6] J. Wang, H. Chen, H. Zhou, X. Liu, W. Qiao, D. Long, L. Ling, Carbon dioxide capture using polyethylenimine-loaded mesoporous carbons, J. Environ. Sci. China (China) 25 (1) (2013) 124–132.
[7] N. Thouchprasitchai, N. Pintuyothin, S. Pongstabodee, Optimization of CO2 adsorption capacity and cyclical adsorption/desorption on tetraethylenepentamine-supported surface-modified hydrotalcite, J. Environ. Sci. China (China) 65 (2018) 293–305.
[8] J. Elfving, C. Bajamundi, J. Kauppinen, T. Sainio, Modelling of equilibrium working capacity of PSA, TSA and TVSA processes for CO2 adsorption under direct air capture conditions, J. CO2 Util. 22 (2017) 270–277.
[9] Y. Meng, J. Jiang, Y. Gao, F. Yan, N. Liu, A. Aihemaiti, Comprehensive study of CO2 capture performance under a wide temperature range using polyethyleneimine-modified adsorbents, J. CO2 Util. 27 (2018) 89–98.
[10] R.R. Kondakindi, G. McCumber, S. Aleksic, W. Whittenberger, M.A. Abraham, Na2CO3-based sorbents coated on metal foil: CO2 capture performance, Int. J. Greenh. Gas Control 15 (2013) 65–69.
[11] A. Jayakumar, A. Gomez, N. Mahinpey, Post-combustion CO2 capture using solid K2CO3: discovering the carbonation reaction mechanism, Appl. Energy 179 (2016) 531–543.
[12] V.S. Derevschikov, J.V. Veselovskaya, T.Y. Kardash, D.A. Trubitsyn, A.G. Okunev, Direct CO2 capture from ambient air using K2CO3/Y2O3 composite sorbent, Fuel 127 (2014) 212–218.
[13] J.V. Veselovskaya, V.S. Derevschikov, T.Y. Kardash, O.A. Stonkus, T.A. Trubitsina, A.G. Okunev, Direct CO2 capture from ambient air using K2CO3/Al2O3 composite sorbent, Int. J. Greenh. Gas Control 17 (2013) 332–340.
[14] C. Zhao, Y. Guo, C. Li, S. Lu, Removal of low concentration CO2 at ambient temperature using several potassium-based sorbents, Appl. Energy 124 (2014) 241–247.
[15] Y. Guo, C. Zhao, C. Li, Y. Wu, CO2 sorption and reaction kinetic performance of K2CO3/AC in low temperature and CO2 concentration, Chem. Eng. J. 260 (2015) 596–604.
[16] R. Rodríguez-Mosqueda, E.A. Bramer, G. Brem, CO2 capture from ambient air using hydrated Na2CO3 supported on activated carbon honeycombs with application to CO2 enrichment in greenhouses, Chem. Eng. Sci. 189 (2018) 114–122.
[17] R. Rodríguez-Mosqueda, E.A. Bramer, T. Roestenberg, G. Brem, Parametrical study on CO2 capture from ambient air using hydrated K2CO3 supported on an activated carbon honeycomb, Ind. Eng. Chem. Res. 57 (10) (2018) 3628–3638.
[18] D.D. Do, S. Junpirom, H.D. Do, A new adsorption–desorption model for water adsorption in activated carbon, Carbon 47 (6) (2009) 1466–1473.
[19] L. Greenspan, Humidity fixed points of binary saturated aqueous solutions, J. Res. Natl. Bur. Stand. Sect. A 81A (1) (1977) 89–96.
[20] C.E. Vanderzee, D.A. Wigg, The standard enthalpies of solution and formation of Wegscheider's salt: Na2CO3 · 3NaHCO3(s) and of trona: Na2CO3 · NaHCO3 · 2H2O (s) at 298.15 K, J. Chem. Thermodyn. 13 (6) (1981) 573–583.
[21] S. Toan, W. O'Dell, C.K. Russell, S. Zhao, Q. Lai, H. Song, Y. Zhao, M. Fan, Thermodynamics of NaHCO3 decomposition during Na2CO3-based CO2 capture, J. Environ. Sci. China (China) (2018).
[22] Y. Duan, D.R. Luebke, H.W. Pennline, B. Li, M.J. Janik, J.W. Halley, Ab initio thermodynamic study of the CO2 capture properties of potassium carbonate sesquihydrate, K2CO3·1.5H2O, J. Phys. Chem. C 116 (27) (2012) 14461–14470.
[23] H. Tanaka, Comparison of thermal properties and kinetics of decompositions of NaHCO3 and KHCO3, J. Therm. Anal. 32 (1987) 521–526.
[24] A. De Gelder, J.A. Dieleman, G.P.A. Bot, L.F.M. Marcelis, An overview of climate and crop yield in closed greenhouses, J. Hortic. Sci. Biotechnol. 87 (3) (2012) 193–202.
[25] Blom, T. J.; Straver, W. A.; Ingratta, F. J.; Khosla, S. OMAFRA Factsheet Carbon Dioxide in Greenhouses. http://www.omafra.gov.on.ca/english/crops/facts/00-077.htm Accessed on October 2018.
[26] T. Qian, J.A. Dieleman, A. Elings, A. De Gelder, L.F.M. Marcelis, O. Van Kooten, In Comparison of Climate and Production in Closed, Semi-Closed and Open Greenhouses, Acta Hortic. 893, 2011, International Society for Horticultural Science (ISHS), Leuven, Belgium, 2011, pp. 807–814.
[27] S.-H. Yang, C.G. Lee, A. Ashtiani-Araghi, J.Y. Kim, J.Y. Rhee, Development and evaluation of combustion-type CO2 enrichment system connected to heat pump for greenhouses, EAEF 7 (1) (2014) 28–33.
[28] H. Umeda, D.-H. Ahn, Y. Iwasaki, S. Matsuo, S. Takeya, A cooling and CO2 enrichment system for greenhouse production using CO2 clathrate hydrate, EAEF 8 (4) (2015) 307–312.
[29] J. Bao, W.-H. Lu, J. Zhao, X.T. Bi, Greenhouses for CO2 sequestration from atmosphere, Carbon Resour. Convers. 1 (2) (2018) 183–190.